Parton transport and hadronization from the dynamical quasiparticle point of view

W. Cassing[1] and E. L. Bratkovskaya[2]
[1]*Institut für Theoretische Physik, Universität Giessen, D-35392 Giessen, Germany*
[2]*Frankfurt Institute for Advanced Studies, JWG Universität Frankfurt, D-60438 Frankfurt am Main, Germany*
(Received 6 April 2008; revised manuscript received 31 July 2008; published 29 September 2008)

The hadronization of an expanding partonic fireball is studied within the parton-hadron-string-dynamics (PHSD) approach, which is based on a dynamical quasiparticle model (DQPM) matched to reproduce lattice QCD results in thermodynamic equilibrium. Apart from strong parton interactions, the expansion and development of collective flow is driven by strong gradients in the parton mean fields. An analysis of the elliptic flow v_2 demonstrates a linear correlation with the spatial eccentricity ϵ as in ideal hydrodynamics. The hadronization occurs by quark-antiquark fusion or three-quark/three-antiquark recombination, which is described by covariant transition rates. Since the dynamical quarks become very massive, the formed resonant "pre-hadronic" color-dipole states ($q\bar{q}$ or qqq) are of high invariant mass, too, and sequentially decay to the ground-state meson and baryon octets increasing the total entropy. This solves the entropy problem in hadronization in a natural way. The resulting particle ratios turn out to be in line with those from a grand-canonical partition function at temperature $T \approx 170$ MeV rather independent from the initial temperature and indicate an approximate strangeness equilibration.

DOI: 10.1103/PhysRevC.78.034919 PACS number(s): 25.75.−q, 13.60.Le, 14.40.Lb, 14.65.Dw

I. INTRODUCTION

The big-bang scenario implies that in the first microseconds of the universe, the entire state emerged from a partonic system of quarks, antiquarks, and gluons—a quark-gluon plasma (QGP)—to color-neutral hadronic matter consisting of interacting hadronic states (and resonances) in which the partonic degrees of freedom are confined. The nature of confinement and the dynamics of this phase transition have motivated a large community for several decades and is still an outstanding question of today's physics. Early concepts of the QGP were guided by the idea of a weakly interacting system of partons which might be described by perturbative QCD (pQCD). However, experimental observations at the BNL Relativistic Heavy Ion Collider (RHIC) indicated that the new medium created in ultrarelativistic Au+Au collisions was interacting more strongly than hadronic matter (cf. Ref. [1] and references therein), and consequently this concept had to be given up. Moreover, in line with the theoretical studies in Refs. [2–4], the medium showed phenomena of an almost perfect liquid of partons [5,6] as extracted from the strong radial expansion and elliptic flow of hadrons [5].

The question about the properties of this (nonperturbative) QGP liquid is discussed controversially in the literature, and dynamical concepts describing the formation of color-neutral hadrons from partons are scarce [7–13]. A fundamental issue for hadronization models is the conservation of four-momentum as well as the entropy problem, because by fusion/coalescence of massless (or low constituent mass) partons to color-neutral bound states of low invariant mass (e.g., pions), the number of degrees of freedom and thus the total entropy is reduced in the hadronization process [9–11]. This problem—a violation of the second law of thermodynamics as well as of the conservation of four-momentum and flavor currents—definitely needs a sound dynamical solution.

A consistent dynamical approach—valid also for strongly interacting systems—can be formulated on the basis of Kadanoff-Baym (KB) equations [14,15] or off-shell transport equations in phase-space representation, respectively [15–17]. In the KB theory, the field quanta are described in terms of propagators with complex self-energies. Whereas the real part of the self-energies can be related to mean-field potentials, the imaginary parts provide information about the lifetime and/or reaction rates of time-like "particles" [4]. Once the proper (complex) self-energies of the degrees of freedom are known, the time evolution of the system is fully governed by off-shell transport equations (as described in Refs. [15–17]).

The determination/extraction of complex self-energies for the partonic degrees of freedom has been performed in Refs. [4,18,19] by fitting lattice QCD (lQCD) "data" within the dynamical quasiparticle model (DQPM). In fact, the DQPM allows a simple and transparent interpretation of lattice QCD results for thermodynamic quantities as well as correlators and leads to effective strongly interacting partonic quasiparticles with broad spectral functions. We stress that mean-field potentials for the "quarks" and "gluons" as well as effective interactions have been extracted from lQCD within the DQPM as well (cf. Ref. [19]).

II. THE PHSD APPROACH

The parton-hadron-string-dynamics (PHSD) approach is a microscopic covariant transport model that incorporates effective partonic as well as hadronic degrees of freedom and involves a dynamical description of the hadronization process from partonic to hadronic matter. Whereas the hadronic part is essentially equivalent to the conventional hadron-string-dynamics (HSD) approach [20], the partonic dynamics is based on the DQPM [18,19], which describes QCD properties in

terms of single-particle Green's functions [in the sense of a two-particle irreducible (2PI) approach].

A. Reminder of the DQPM

We briefly recall the basic assumptions of the DQPM. Following Ref. [21], the dynamical quasiparticle mass (for gluons and quarks) is assumed to be given by the thermal mass in the asymptotic high-momentum regime, which is proportional to the coupling $g(T/T_c)$ and the temperature T with a running coupling (squared), that is,

$$g^2(T/T_c) = \frac{48\pi^2}{(11N_c - 2N_f)\ln[\lambda^2(T/T_c - T_s/T_c)^2]}. \quad (1)$$

Here $N_c = 3$ stands for the number of colors, while N_f denotes the number of flavors. The parameters controlling the infrared enhancement of the coupling $\lambda = 2.42$ and $T_s = 0.46T_c$ have been fitted in Ref. [21] to lQCD results for the entropy density $s(T)$. An almost perfect reproduction of the energy density $\varepsilon(T)$ and the pressure $P(T)$ from lQCD is achieved as well. As demonstrated in Fig. 1 of Ref. [19], this functional form for the strong coupling $\alpha_s = g^2/(4\pi)$ is in full accordance with the lQCD calculations of Ref. [22] for the long-range part of the $q - \bar{q}$ potential, too.

The width for gluons and quarks (for vanishing chemical potential μ_q) is adopted in the form [23]

$$\gamma_g(T) = \frac{3g^2T}{8\pi}\ln\left(\frac{2c}{g^2}\right), \quad \gamma_q(T) = \frac{g^2T}{6\pi}\ln\left(\frac{2c}{g^2}\right), \quad (2)$$

where $c = 14.4$ (from Ref. [4]) is related to a magnetic cutoff. We stress that a nonvanishing width γ is the central difference of the DQPM from conventional quasiparticle models [24–26]. Its influence is essentially seen in correlation functions as, e.g., in the stationary limit of the correlation function in the off-diagonal elements of the energy-momentum tensor T^{kl} which defines the shear viscosity η of the medium [4,27]. Here a sizable width is mandatory to obtain a small ratio in the shear viscosity to entropy density η/s.

In line with Ref. [21], the parton spectral functions thus are no longer $\delta-$ functions in the invariant mass squared but taken as

$$\rho_j(\omega) = \frac{\gamma_j}{E_j}\left(\frac{1}{(\omega - E_j)^2 + \gamma_j^2} - \frac{1}{(\omega + E_j)^2 + \gamma_j^2}\right) \quad (3)$$

separately for quarks and gluons ($j = q, \bar{q}, g$). With the convention $E^2(\boldsymbol{p}) = \boldsymbol{p}^2 + M_j^2 - \gamma_j^2$, the parameters M_j^2 and γ_j are directly related to the real and imaginary parts of the retarded self-energy, e.g., $\Pi_j = M_j^2 - 2i\gamma_j\omega$.

With the spectral functions fixed by Eqs. (1)–(3), the total energy density in the DQPM (at vanishing quark chemical potential) can be evaluated as

$$T^{00} = d_g\int_0^\infty \frac{d\omega}{2\pi}\int\frac{d^3p}{(2\pi)^3}2\omega^2\rho_g(\omega,\mathbf{p})n_B(\omega/T) + d_q\int_0^\infty\frac{d\omega}{2\pi}\int\frac{d^3p}{(2\pi)^3}2\omega^2\rho_q(\omega,\mathbf{p})n_F(\omega/T), \quad (4)$$

where n_B and n_F denote the Bose and Fermi functions, respectively. The number of transverse gluonic degrees of freedom is $d_g = 16$, while the fermic degrees of freedom amount to $d_q = 4N_cN_f = 36$ in the case of three flavors ($N_f = 3$). The pressure P then may be obtained by integrating the differential thermodynamic relation

$$P - T\frac{\partial P}{\partial T} = -T^{00}, \quad (5)$$

with the entropy density s given by

$$s = \frac{\partial P}{\partial T} = \frac{T^{00} + P}{T}. \quad (6)$$

This approach is thermodynamically consistent and represents a 2PI approximation to hot QCD, once the free parameters in Eqs. (1) and (2) are fitted to lattice QCD results as in Refs. [4,18,19].

As outlined in detail in Refs. [18,19], the energy density functional (4) can be separated in space-like and time-like sectors when the spectral functions acquire a finite width. The space-like part of Eq. (4) defines a potential energy density V_p, since the field quanta involved are virtual and correspond to partons exchanged in interaction diagrams. The time-like part of Eq. (4) corresponds to effective field quanta which can be propagated within the light-cone. Related separations can be made for virtual and time-like parton densities [18,19]. Without repeating the details, we mention that mean-field potentials for partons can be defined by the derivative of the potential energy density V_p with respect to the time-like parton densities and effective interactions by second derivatives of V_p (cf. Sec. III in Ref. [19]).

B. Hadronization in PHSD

Based on the DQPM, we have developed an off-shell transport approach denoted as PHSD, where the degrees of freedom are dynamical quarks, antiquarks, and gluons ($q, \bar{q}, g$) with rather large masses and broad spectral functions in line with Eqs. (1)–(3) as well as the conventional hadrons (described in the standard HSD approach [20]). On the partonic side, the following elastic and inelastic interactions are included: $qq \leftrightarrow qq, \bar{q}\bar{q} \leftrightarrow \bar{q}\bar{q}, gg \leftrightarrow gg, gg \leftrightarrow g$, and $q\bar{q} \leftrightarrow g$, exploiting "detailed balance" with interaction rates from the DQPM [4,18,19] (cf. Sec. III B). The hadronization, i.e., transition from partonic to hadronic degrees of freedom, is described by local covariant transition rates; e.g., for $q + \bar{q}$ fusion to a meson m of four-momentum $p = (\omega, \mathbf{p})$ at space-time point $x = (t, \mathbf{x})$,

$$\frac{dN_m(x,p)}{d^4xd^4p} = Tr_qTr_{\bar{q}}\,\delta^4(p - p_q - p_{\bar{q}})\,\delta^4\left(\frac{x_q + x_{\bar{q}}}{2} - x\right) \times \omega_q\rho_q(p_q)\omega_{\bar{q}}\rho_{\bar{q}}(p_{\bar{q}})|v_{q\bar{q}}|^2 \times W_m(x_q - x_{\bar{q}}, p_q - p_{\bar{q}})N_q(x_q, p_q) \times N_{\bar{q}}(x_{\bar{q}}, p_{\bar{q}})\,\delta(\text{flavor, color}). \quad (7)$$

In Eq. (7), we have introduced the shorthand notation

$$Tr_j = \sum_j\int d^4x_jd^4p_j/(2\pi)^4, \quad (8)$$

where $\sum_j$ denotes a summation over discrete quantum numbers (spin, flavor, color); $N_j(x, p)$ is the phase-space density of parton j at space-time position x and four-momentum p. In Eq. (7), δ(flavor, color) stands symbolically for the conservation of flavor quantum numbers as well as color neutrality of the formed hadron m, which can be viewed as a color-dipole or pre-hadron. Furthermore, $v_{q\bar{q}}(\rho_p)$ is the effective quark-antiquark interaction from the DQPM defined by Eq. (31) and displayed in Fig. 10 of Ref. [19] as a function of the local parton $(q + \bar{q} + g)$ density ρ_p (or energy density). Furthermore, $W_m(x, p)$ is the phase-space distribution of the formed pre-hadron. It is taken as a Gaussian in coordinate and momentum space (following Ref. [28]) with width $\sqrt{\langle r^2 \rangle} = 0.66$ fm (in the rest frame), which corresponds to an average rms radius of mesons. The width in momentum space is fixed by the uncertainty principle, i.e., $\Delta x \Delta p = 1$ (in natural units). We note that the final hadron formation rates are approximately independent on these parameters within reasonable variations.

In principle, the two-particle Green's function $G^<(x_q, p_q, x_{\bar{q}}, p_{\bar{q}})$ should appear in Eq. (7). The approximation of the two-particle Green's function by a (symmetrized/antisymmetrized) product of single-particle Green's functions is always a first step in a cluster expansion for Green's functions and neglects "residual correlations" stemming from higher order contractions. The same holds for an approximation of the three-particle Green's function by the (symmetrized/antisymmetrized) product of single-particle Green's functions (cf. Ref. [29]). However, the DQPM with its dynamical spectral functions already includes the effects of strong two-body correlations—contrary to bare Green's functions—such that the effect of residual interactions might be discarded in a first approximation. But there is no *a priori* guarantee that this approximation is appropriate under all circumstances. This, in principle, should be examined by lattice QCD in order to test the cluster decomposition in hot QCD.

Related transition rates [to Eq. (7)] are defined for the fusion of three off-shell quarks $(q_1 + q_2 + q_3 \leftrightarrow B)$ to color-neutral baryonic (B or $\bar{B}$) resonances of finite width (or strings) fulfilling energy and momentum conservation as well as flavor current conservation, i.e.,

$$\begin{aligned}\frac{dN_B(x,p)}{d^4x d^4p} &= Tr_{q_1} Tr_{q_2} Tr_{q_3} \delta^4(p - p_1 - p_2 - p_3) \\ &\times \delta^4\left(\frac{x_{q_1} + x_{q_2} + x_{q_3}}{3} - x\right) \\ &\times \omega_{q_1}\rho_{q_1}(p_1)\omega_{q_2}\rho_{q_2}(p_2)\,\omega_{q_3}\rho_{q_3}(p_3) \\ &\times |M_{qqq}|^2 W_B(x_1, x_2, x_3, p_1, p_2, p_3) \\ &\times N_{q_1}(x_1, p_1) N_{q_2}(x_2, p_2) N_{q_3}(x_3, p_3)\,\delta(\text{flavor, color}). \quad (9)\end{aligned}$$

Here, the quantity W_B denotes the baryon phase-space distribution (evaluated in Jacobi coordinates), which is taken again of Gaussian shape with a width of 1 fm in coordinate space which corresponds to an average rms radius of excited baryons. The matrix element squared $|M_{qqq}|^2$ reflects the strength of three-quark fusion processes and is fixed as follows. Since Regge trajectories for excited mesonic and baryonic states have the same slope (or string constant in the color dipole picture), we tentatively set $|M_{qqq}|^2 = |v_{q\bar{q}}|^3$ in our present work, which implies that (so far) there is no need to introduce any new parameter.

On the hadronic side, PHSD includes explicitly the baryon octet and decouplet, the 0^- and 1^- meson nonets as well as selected higher resonances as in HSD [20]. Hadrons of higher masses (>1.5 GeV for baryons and >1.3 GeV for mesons) are treated as "strings" (color dipoles) that decay to the known (low mass) hadrons according to the JETSET algorithm [30].

III. HADRONIZATION OF AN EXPANDING PARTONIC FIREBALL

We now turn to actual results from PHSD for the model case of an expanding partonic fireball at initial temperature $T = 1.7T_c$ ($T_c = 0.185$ GeV) with quasiparticle properties and four-momentum distributions determined by the DQPM at temperature $T = 1.7T_c$.

A. Initial conditions

The initial distribution for quarks, antiquarks, and gluons in coordinate space is taken as a Gaussian ellipsoid with a spatial eccentricity

$$\epsilon = \langle y^2 - x^2 \rangle / \langle y^2 + x^2 \rangle, \quad (10)$$

and $\langle z^2 \rangle = \langle y^2 \rangle$ in order to allow for the buildup of elliptic flow (as in semicentral nucleus-nucleus collisions at relativistic energies). To match the initial off-equilibrium strange quark content in relativistic pp collisions, the number of s (and $\bar{s}$ quarks) is assumed to be suppressed by a factor of 3 relative to the abundance of u and d quarks and antiquarks. In this way, we will be able to investigate additionally the question of strangeness equilibration.

As mentioned above, the dynamical evolution of the system is then entirely described by the transport dynamics in PHSD incorporating the off-shell propagation of the partonic quasiparticles according to Ref. [16] as well as the transition to resonant hadronic states (or strings) in Eqs. (7) and (9). The time integration for the test particle equations of motion (cf. Ref. [16]) is performed in the same way as for hadronic off-shell transport, where (in view of the momentum-independent width γ) the simple relation (19) in Ref. [31] is employed. For the collisions of partons, two variants are at our disposal: (i) geometric collision criteria as employed in standard hadronic transport and ii) the in-cell method developed in Ref. [32]. The latter can easily be extended to describe $2 \leftrightarrow 3$ processes, etc., in a covariant way [33] and is the better choice at high-particle densities (cf. Ref. [34]). The hadronization is performed by integrating the rate equations (7) and (9) in space and time which are discretized by Δt and $\Delta V(t)$. We use local cells of volume $dV(t) = 0.25(1 + bt)^3$ fm^3, where t is given in units of fm/c and $b = 0.025\,c$/fm. This choice approximately corresponds to a comoving grid for the expanding system. In each time-step Δt and cell ΔV, the integrals in Eqs. (7) and (9) are evaluated by a sum over all (time-like) test particles,

using (e.g., for the quark density)

$$\frac{1}{\Delta V}\int_{\Delta V} d^3x \int \frac{d\omega_q}{2\pi}\omega_q \int \frac{d^3p_q}{(2\pi)^3}\,\rho_q(\omega_q, p_q)N_q(x, p_q) = \frac{1}{\Delta V}\sum_{J_q \varepsilon \Delta V} 1 = \rho_q(\Delta V), \tag{11}$$

where the sum over J_q implies a sum over all test particles of type q (here quarks) in the local volume ΔV in each parallel run. To obtain lower fluctuations, the integrals are averaged over the number of parallel runs (typically a few hundred). For each individual test particle (i.e., x_q and p_q fixed), the additional integrations in Eqs. (7) and (9) give a probability for a hadronization process to happen; the actual event then is selected by Monte Carlo. Since energy-momentum conservation fixes the four-momentum p of the hadron produced—the space-time position x is fixed by Eqs. (7) or (9)—the latter is represented by a hadronic state with flavor content fixed by the fusing quarks (antiquarks). The latter decays to the lower mass hadrons according to JETSET [30] above thresholds of 1.3 GeV for mesonic states or 1.5 GeV for baryonic states (as in HSD). Lower mass hadrons (octet and decuplet states) are determined by the weight of their respective spectral functions at given invariant mass and selected by Monte Carlo. Note that the propagation of partons includes the space-time derivatives of the quark and gluon mean fields specified in Eq. (29) and displayed in Fig. 9 of Ref. [19].

B. Dynamical evolution

In Fig. 1(a), we show the energy balance for the expanding system at initial temperature $T = 1.7T_c$ and eccentricity $\epsilon = 0$, i.e., a fireball of spherical symmetry. The total energy $E_{\rm tot}$—which at $t = 0$ is given by Eq. (4) integrated over space—is conserved within 3% throughout the partonic expansion and hadronization phase such that for $t > 8$ fm/c, it is given essentially by the energy contribution from mesons and baryons (+antibaryons). The initial energy splits into the partonic interaction energy V_p [cf. Eq. (19) in Ref. [19]] and the energy of the time-like (propagating) partons

$$T_p = \sum_i \sqrt{p_i^2 + M_i^2(\rho_p)}, \tag{12}$$

with fractions determined by the DQPM [19]. In Eq. (12) the summation over i runs over all test particles in an individual run. The hadronization mainly proceeds during the time interval $1 < t < 7$ fm/c [cf. Fig. 1(b) where the time evolutions of the q, $\bar{q}$, g, meson, and baryon (+antibaryon) numbers are displayed].

As one observes from Fig. 1, on average the number of hadrons from the resonance or string decays is larger than the initial number of fusing partons. This might be astonishing, since by partonic fusion the number of final states is conventionally reduced in coalescence models.

To shed some light on the hadronization process in PHSD, we display in Fig. 2 the invariant mass distribution of $q\bar{q}$ pairs (solid line) as well as qqq (and $\bar{q}\bar{q}\bar{q}$) triples (dashed line) that lead to the formation of final hadronic states. In fact, the distribution for the formation of baryon (antibaryon) states starts above the nucleon mass and extends to high invariant mass covering the nucleon resonance mass region as well as the high mass continuum (which is treated by the decay of strings within the JETSET model [30]). On the "pre-mesonic" side, the invariant-mass distribution starts roughly above the

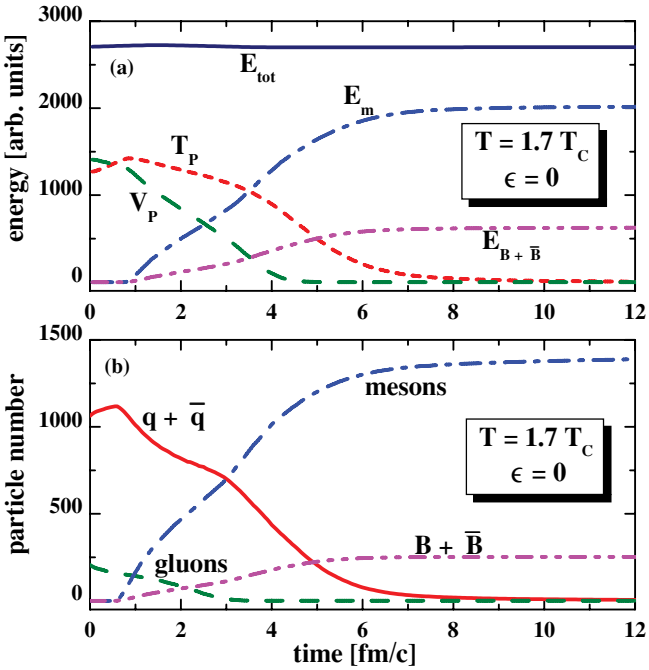

FIG. 1. (Color online) (a) Time evolution of the total energy $E_{\rm tot}$ (upper line), the partonic contributions from the interaction energy V_p and the energy of time-like partons T_p in comparison to the energy contribution from formed mesons E_m and baryons (+antibaryons) $E_{B+\bar{B}}$. (b) Time evolution in the parton, meson, and baryon numbers for an expanding partonic fireball at initial temperature $T = 1.7T_c$ with initial eccentricity $\epsilon = 0$.

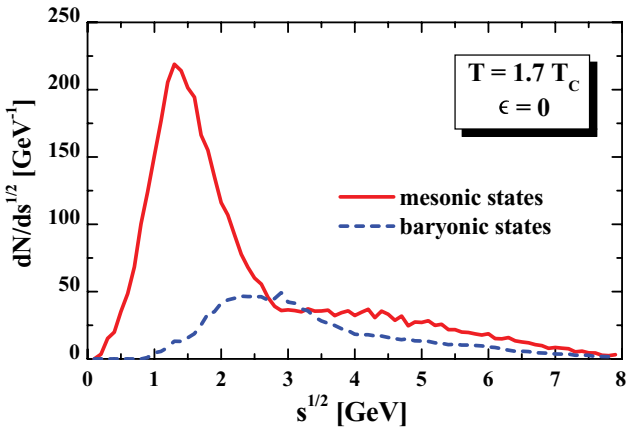

FIG. 2. (Color online) Invariant mass distribution for fusing $q\bar{q}$ pairs (solid line) as well as qqq ($\bar{q}\bar{q}\bar{q}$) triples (dashed line) that lead to the formation of final hadronic states for an expanding partonic fireball at initial temperature $T = 1.7T_c$ with initial eccentricity $\epsilon = 0$.

two-pion mass and extends up to continuum states of high invariant mass (described again in terms of string excitations). The low mass sector is dominated by ρ, a_1, ω or $K^*, \bar{K}^*$ transitions etc. The excited "pre-hadronic" states decay to two or more "pseudoscalar octet" mesons such that the number of final hadrons is larger than the initial number of fusing partons.

Accordingly, the hadronization process in PHSD leads to an increase of the total entropy and not to a decrease as in the coalescence models [9,10]. This is a direct consequence of the finite (and rather large) dynamical quark and antiquark masses as well as mean-field potentials which—by energy conservation—lead to pre-hadron masses well above those for the pseudoscalar meson octet or the baryon octet, respectively. This solves the entropy problem in hadronization in a natural way and is in accordance with the second law of thermodynamics!

The parton dynamics itself is governed by their propagation in the time-dependent mean-field $U_p(\rho_p)$, which is adopted in the parametrized form (as a function of the parton density ρ_p) given by Eq. (29) in Ref. [19]. Since the mean-field U_p is repulsive, the partons are accelerated during the expansion phase at the expense of the potential energy density V_p, which is given by the integral of U_p over ρ_p (cf. Sec. III in Ref. [19]). The interaction rates of the partons are determined by effective cross sections, which for gg scattering have been determined in Ref. [4] as a function of T/T_c. The latter are reparametrized in the actual calculation as a function of the parton density using the available dependence of $\rho_p(T)$ on the temperature T from the DQPM.

The actual values for gg scattering are shown in Fig. 3 as a function of the parton density ρ_p (solid line) and demonstrate that gg cross sections up to 20 mb can be reached at $\rho_p \approx 2.5$ fm^{-3}. The effective cross section drops rapidly with increasing ρ_p which signals that weakly interacting partons might show up at very high parton density. Some note of caution has to be added here since though the cross section σ_{gg} drops with ρ_p the collision rate of a gluon ($\sim\sigma_{gg}\rho_p$) increases slightly with ρ_p. For quark-quark or quark-antiquark elastic scattering, the cross section is reduced by a factor 4/9 in line

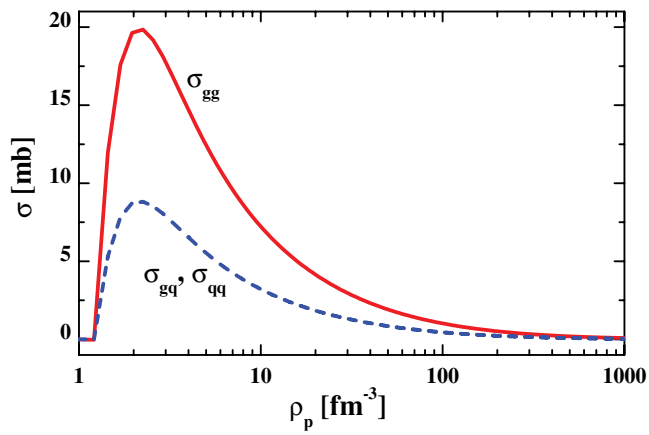

FIG. 3. (Color online) Effective gluon-gluon → gluon-gluon (solid line), gluon-quark → gluon-quark and quark-quark → quark-quark (dashed line) cross sections from the DQPM as a function of the parton density ρ_p.

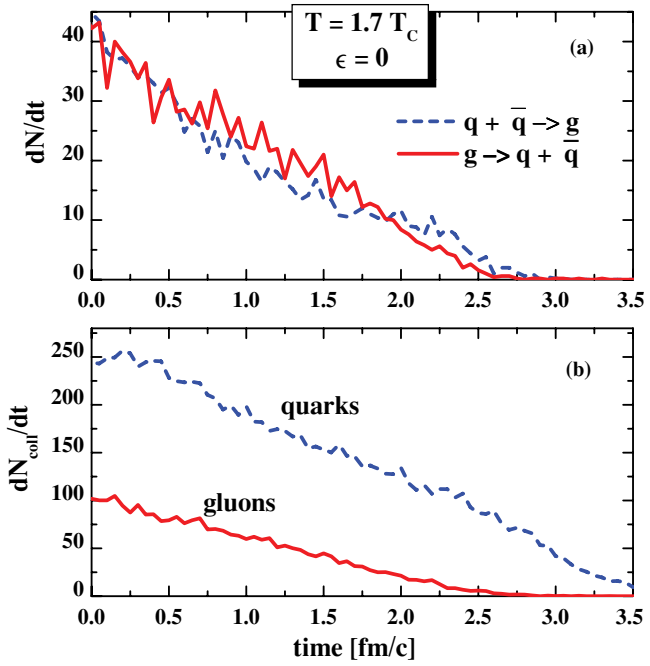

FIG. 4. (Color online) (a) Interaction rate for the channels $q + \bar{q} \to g$ and $g \to q + \bar{q}$ for an expanding partonic fireball at initial temperature $T = 1.7T_c$ with initial eccentricity $\epsilon = 0$. (b) Collision rate of gluons and quarks or antiquarks.

with Casimir scaling. Quark-gluon elastic scattering (in the present implementation) is also reduced by a factor of 4/9 (cf. Fig. 3, dashed line). The channels $q\bar{q} \to g$ are described by a relativistic Breit-Wigner cross section, which is determined by the actual masses of the fermions, the invariant energy $\sqrt{s}$, and the resonance parameters of the gluon (from the DQPM). In this case, a further constraint on flavor neutrality and open color is employed. The gluon decay to a $u\bar{u}$, $d\bar{d}$, or $s\bar{s}$ pair is fixed by detailed balance. Further channels are $gg \leftrightarrow g$, which are given by Breit-Wigner cross sections (with the gluon resonance parameters) and detailed balance, respectively.

The actual interaction rates for the channels $q + \bar{q} \to g$ and $g \to q + \bar{q}$ are displayed in Fig. 4(a) for the expanding partonic fireball at initial temperature $T = 1.7T_c$ with initial eccentricity $\epsilon = 0$. Within statistics, the numerical result shows that detailed balance actually is fulfilled for the expanding partonic system which was initialized in thermal equilibrium. Figure 4(b) shows the total number of collisions per time for gluons and for quarks or antiquarks, which is higher for the fermions since the latter are much more frequent than the gluons.

Let's also have a look at the transverse momentum p_T spectra of hadrons emerging from the PHSD dynamics of the expanding fireball initialized with $T = 1.7T_c$. The resulting p_T spectra are displayed in Fig. 5(a) for pions and nucleons and show that the nucleons become more abundant for $p_T > 2.5$ GeV/c. The ratio of nucleons to pions is depicted in Fig. 5(b) and clearly demonstrates that baryons (antibaryons) become more frequent than mesons at high $p_T > 2.5$ GeV. This observation is in close analogy to the experimental findings in Au+Au collisions at top RHIC energies [5].

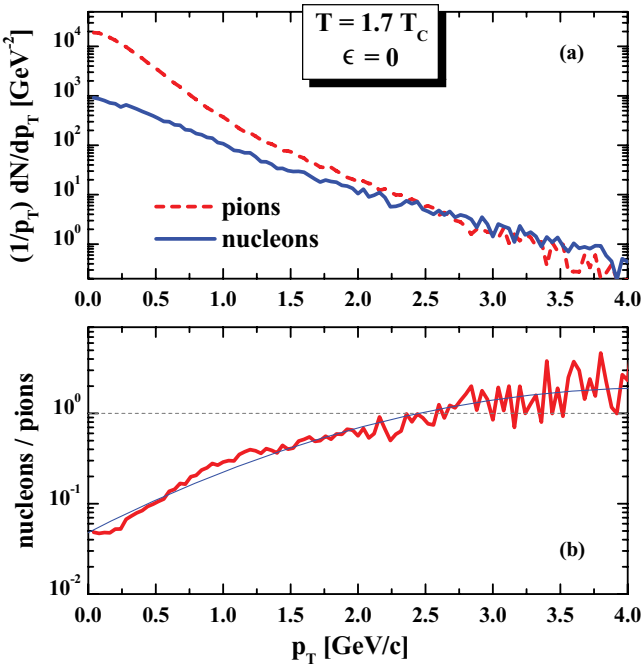

FIG. 5. (Color online) (a) Transverse momentum spectra $(1/p_T)dN/dp_T$ for pions and nucleons for an expanding partonic fireball at initial temperature $T = 1.7T_c$ with initial eccentricity $\epsilon = 0$. (b) Nucleon to pion ratio as a function of the transverse momentum p_T corresponding to the spectra in (a). The thin blue line is drawn to guide the eye because of the limited statistics of the PHSD calculation.

Note that a quantitative comparison with RHIC data is not meaningful because of the rather simplified and special initial conditions employed here.

C. Comparison with the statistical hadronization model

It is also interesting to examine the final particle ratios K^+/π^+, p/π^+, Λ/K^+, etc. (after hadronic decays), which are shown in Table I. The latter ratios are compared with the grand-canonical statistical hadronization model (SM) [35–37] at baryon chemical potential $\mu_B = 0$. For $\mu_B = 0$, the particle ratios depend only on temperature T, and one may fix a freeze-out temperature, e.g., by the proton to π^+ ratio. A respective comparison is given also in Table I for $T = 160$ and 170 MeV for the SM, which demonstrates that the results from PHSD are close to those from the SM for $T \approx 170$ MeV. This also holds roughly for the Λ/K^+ ratio. On the other hand the K^+/π^+ ratio only smoothly depends on temperature T

TABLE I. Comparison of particle ratios from PHSD with the statistical model (SM) [37] for $T = 160$ and 170 MeV.

	p/π^+	Λ/K^+	K^+/π^+
PHSD	0.086	0.28	0.157
SM, $T = 160$ MeV	0.073	0.22	0.179
SM, $T = 170$ MeV	0.086	0.26	0.180

and measures the amount of strangeness equilibration. Recall that we initialized the system with a relative strangeness suppression factor of 1/3. The deviation from the SM ratio by about 13% indicates that strangeness equilibration is not fully achieved in the calculations. This is expected, since the partons in the surface of the fireball hadronize before chemical equilibration may occur. A detailed discussion of results will be presented in a forthcoming study.

The agreement between the PHSD and SM results for the baryon to meson ratio in the strangeness $S = 0$ and $S = 1$ sector may be explained as follows. Since the final hadron formation dominantly proceeds via resonance and string formation and decay—which is approximately a microcanonical statistical process [38]—the average over many hadronization events with different energy/mass and particle number (in the initial and final state) leads to a grand-canonical ensemble. The latter (for $\mu_B = 0$) is only characterized by the average energy or an associated Lagrange parameter $\beta = 1/T$.

D. Elliptic flow

Of additional interest are the collective properties of the partonic system during the early time evolution. To demonstrate the buildup of elliptic flow, we show in Fig. 6 the time evolution of

$$v_2 = \langle (p_x^2 - p_y^2)/(p_x^2 + p_y^2) \rangle \tag{13}$$

for partons, mesons, and baryons for an initial eccentricity $\epsilon = 0.33$. As seen from Fig. 6, the partonic flow develops within 2 fm/c, and the hadrons essentially pick up the collective flow from the accelerated partons. The hadron v_2 is smaller than the maximal parton v_2, since by parton fusion the average v_2 reduces and a fraction of hadrons is formed early at the surface of the fireball without a strong acceleration before hadronization. We briefly mention that the reduction of the average hadron elliptic flow essentially is due to the finite parton masses which are larger than the temperature in the hadronization phase. This reduced hadron v_2 is in contrast to the coalescence of massless partons. A more

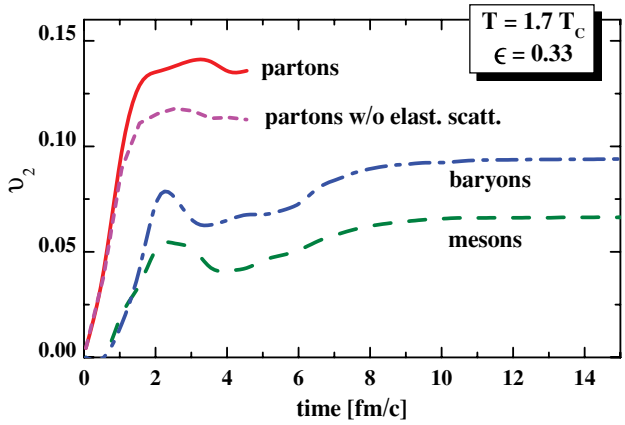

FIG. 6. (Color online) Time evolution of the elliptic flow v_2 for partons and hadrons for the initial spatial eccentricity $\epsilon = 0.33$ for an expanding partonic fireball at initial temperature $T = 1.7T_c$.

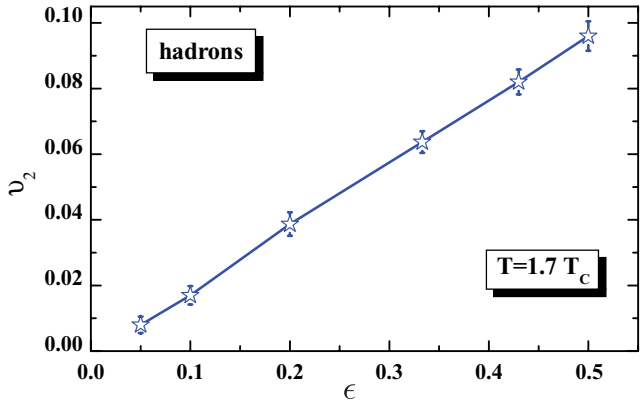

FIG. 7. (Color online) Hadron elliptic flow v_2 vs initial spatial eccentricity ϵ for an expanding partonic fireball at initial temperature $T = 1.7T_c$.

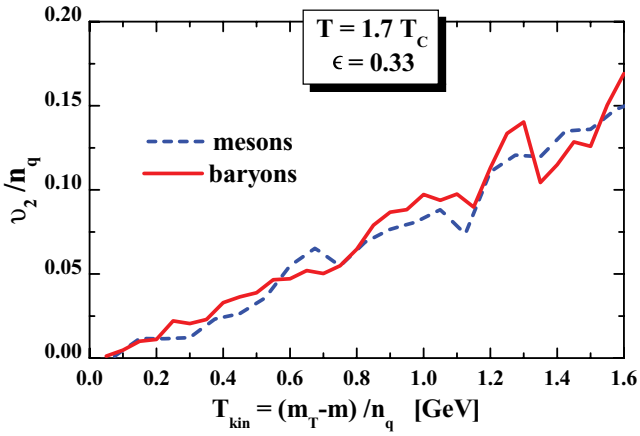

FIG. 8. (Color online) Elliptic flow v_2—scaled by the number of constituent quarks n_q—vs transverse kinetic energy divided by n_q for mesons and baryons.

detailed discussion and investigation of Eqs. (7) and (9) will be presented in an upcoming study.

It is important to point out that in PHSD the elliptic flow of partons predominantly stems from the gradients of the repulsive parton mean fields (from the DQPM) at high parton (energy) density. To demonstrate this statement, we show in Fig. 6 the result of a simulation without elastic partonic rescattering processes (short dashed line).

Figure 7 shows the final hadron v_2 versus the initial eccentricity ϵ and indicates that the ratio v_2/ϵ is practically constant ($\approx$0.2) as in ideal hydrodynamics (cf. Fig. 3 in Ref. [39]). Accordingly, the parton dynamics in PHSD are close to ideal hydrodynamics. This result is expected, since the ratio of the shear viscosity η to the entropy density s in the DQPM is on the level of $\eta/s \approx 0.2$ [4] and thus rather close to the lower bound of $\eta/s = 1/(4\pi)$ [40]. Note that the ratio η/s is dominantly determined by the quasiparticle width γ [Eq. (2)], and low ratios on the level of $\eta/s \approx 0.2$ require broad parton spectral functions as employed in the DQPM.

A further test of the PHSD hadronization approach is provided by the "constituent quark number scaling" of the elliptic flow v_2 which has been observed experimentally in central Au+Au collisions at RHIC [5,41]. In this respect, we plot v_2/n_q versus the transverse kinetic energy per constituent parton,

$$T_{\rm kin} = \frac{m_T - m}{n_q}, \tag{14}$$

with m_T and m denoting the transverse mass and actual mass, respectively. For mesons, we have $n_q = 2$; for baryons/antibaryons, $n_q = 3$. The results for the scaled elliptic flow are shown in Fig. 8 for mesons and baryons and suggest an approximate scaling. We note that the scaled hadron elliptic flow v_2/n_q does not reflect the parton v_2 at hadronization and is significantly smaller. Because of the limited statistics especially in the baryonic sector with increasing p_T, this issue will have to be readdressed with high statistics in the actual heavy-ion case where the very early parton p_T distribution also shows power-law tails.

IV. SUMMARY

In summary, the expansion dynamics of an anisotropic partonic fireball is studied within the PHSD approach, which includes dynamical local transition rates from partons to hadrons [Eqs. (7) and (9)] and vice versa. It shows collective features as expected from ideal hydrodynamics for strongly interacting systems. The hadronization process conserves four-momentum and all flavor currents and slightly increases the total entropy (by about 15% in the model case investigated here), since the "'fusion" of rather massive partons dominantly leads to the formation of color-neutral strings or resonances that decay microcanonically to lower mass hadrons. This solves the entropy problem associated with the simple coalescence model!

We find that the hadron abundances and baryon to meson ratios are compatible with those from the statistical hadronization model [35,36]—which describes well particle ratios from AGS to RHIC energies—at a freeze-out temperature of about 170 MeV. Furthermore, strangeness equilibration is approximately achieved in the dynamical expansion and driven by the processes $q\bar{q} \leftrightarrow g \leftrightarrow s\bar{s}$, which is a resonant process in the DQPM. However, although the final hadron ratios are compatible with a fixed freeze-out temperature ($\sim$170 MeV), we observe that the actual hadronization occurs at very different energy densities (or temperatures) (cf. also Ref. [42]) such that the microscopic studies do not support the sudden freeze-out picture.

Our calculations show that the hadron elliptic flow is essentially produced in the early partonic stage, where also the strong repulsive parton mean fields contribute to a large extent. This might explain why the hadron v_2 from HSD calculations [43] underestimated the RHIC data on v_2 essentially at midrapidity (in the pure hadron/string approach). The hadron elliptic flow from PHSD is smaller than the parton v_2 due to a partial cancellation of the v_2 values from the individual partons in the fusion process to hadrons (but larger than in HSD). This cancellation essentially is a consequence of parton masses that are larger than the local temperature during the hadronization phase. Nevertheless, our observations indicate

an approximate quark number scaling (cf. Fig. 8) for low and moderate transverse kinetic energies within the statistics reached so far. This issue will be followed up in more detail in a forthcoming investigation.

The present study, however, serves only as a model case which allows for a more transparent interpretation of the various results. An application of the PHSD approach to ultrarelativistic heavy-ion collisions, especially in comparison to differential experimental data, is expected to shed further light on the transport properties of the partonic phase and the dynamics of hadronization.

ACKNOWLEDGMENTS

The authors thank A. Andronic for providing the SM results used in Table I and for a critical reading of the manuscript. They are also grateful to O. Linnyk for valuable discussions.

[1] *Quark Matter 2005*, Nucl. Phys. **A774**, 1 (2006); *Quark Matter 2006*, J. Phys. G: Nucl. Part. Phys. **34**, S1 (2007).
[2] E. Shuryak, Prog. Part. Nucl. Phys. **53**, 273 (2004).
[3] M. H. Thoma, J. Phys. G: Nucl. Part. Phys. **31**, L7 (2005).
[4] A. Peshier and W. Cassing, Phys. Rev. Lett. **94**, 172301 (2005).
[5] I. Arsene *et al*., Nucl. Phys. **A757**, 1 (2005); B. B. Back *et al*., *ibid*. **A757**, 28 (2005); J. Adams *et al*., *ibid*. **A757**, 102 (2005); K. Adcox *et al*., *ibid*. **A757**, 184 (2005).
[6] T. Hirano and M. Gyulassy, Nucl. Phys. **A769**, 71 (2006).
[7] A. Ayala, M. Martinez, G. Paic, and G. Toledo Sanchez, Phys. Rev. C **77**, 044901 (2008).
[8] S. Scherer *et al*., New J. Phys. **3**, 8 (2001).
[9] R. C. Hwa and C. B. Yang, Phys. Rev. C **67**, 034902 (2003); V. Greco, C. M. Ko, and P. Levai, Phys. Rev. Lett. **90**, 202302 (2003).
[10] R. J. Fries, B. Müller, C. Nonaka, and S. A. Bass, Phys. Rev. Lett. **90**, 202303 (2003).
[11] Z.-W. Lin, C. M. Ko, B. A. Li, B. Zhang, and S. Pal, Phys. Rev. C **72**, 064901 (2005).
[12] L. Ravagli, H. van Hees, and R. Rapp, arXiv:0806.2055 [hep-ph].
[13] T. S. Biro and K. Urmossy, Eur. Phys. J. ST **155**, 1 (2008).
[14] L. P. Kadanoff and G. Baym, *Quantum Statistical Mechanics* (Benjamin, New York, 1962).
[15] S. Juchem, W. Cassing, and C. Greiner, Phys. Rev. D **69**, 025006 (2004); Nucl. Phys. **A743**, 92 (2004).
[16] W. Cassing and S. Juchem, Nucl. Phys. **A665**, 377 (2000); **A672**, 417 (2000).
[17] Y. B. Ivanov, J. Knoll, and D. N. Voskresensky, Nucl. Phys. **A672**, 313 (2000).
[18] W. Cassing, Nucl. Phys. **A791**, 365 (2007).
[19] W. Cassing, Nucl. Phys. **A795**, 70 (2007).
[20] W. Cassing and E. L. Bratkovskaya, Phys. Rep. **308**, 65 (1999); W. Ehehalt and W. Cassing, Nucl. Phys. **A602**, 449 (1996).
[21] A. Peshier, Phys. Rev. D **70**, 034016 (2004); J. Phys. G: Nucl. Part. Phys. **31**, S371 (2005).
[22] O. Kaczmarek, F. Karsch, F. Zantow, and P. Petreczky, Phys. Rev. D **70**, 074505 (2004); **72**, 059903(E) (2005).
[23] R. D. Pisarski, Phys. Rev. Lett. **63**, 1129 (1989).
[24] A. Peshier, B. Kämpfer, O. P. Pavlenko, and G. Soff, Phys. Rev. D **54**, 2399 (1996); P. Levai and U. Heinz, Phys. Rev. C **57**, 1879 (1998); A. Peshier, B. Kämpfer, and G. Soff, *ibid*. **61**, 045203 (2000); Phys. Rev. D **66**, 094003 (2002).
[25] M. Bluhm, B. Kämpfer, R. Schulze, D. Seipt, and U. Heinz, Phys. Rev. C **76**, 034901 (2007).
[26] J. Letessier and J. Rafelski, Phys. Rev. C **67**, 031902(R) (2003).
[27] G. Aarts and J. M. Martinez Resco, J. High Energy Phys. 04 (2002) 053; 02 (2004) 061.
[28] C. B. Dover, U. Heinz, E. Schnedermann, and J. Zimanyi, Phys. Rev. C **44**, 1636 (1991).
[29] S. J. Wang *et al*., Nucl. Phys. **A573**, 245 (1994).
[30] H.-U. Bengtsson and T. Sjöstrand, Comput. Phys. Commun. **46**, 43 (1987).
[31] E. L. Bratkovskaya and W. Cassing, Nucl. Phys. **A807**, 214 (2008).
[32] A. Lang, H. Babovsky, W. Cassing, U. Mosel, H.-G. Reusch, and K. Weber, J. Comput. Phys. **106**, 391 (1993).
[33] W. Cassing, Nucl. Phys. **A700**, 618 (2002).
[34] Z. Xu and C. Greiner, Phys. Rev. C **71**, 064901 (2005).
[35] P. Braun-Munzinger *et al*., Phys. Lett. **B365**, 1 (1996); **B465**, 15 (1999); **B518**, 41 (2001).
[36] A. Andronic, P. Braun-Munzinger, and J. Stachel, Nucl. Phys. **A772**, 167 (2006).
[37] A. Andronic (private communication).
[38] F. Beccatini, Z. Phys. C **69**, 485 (1996).
[39] S. A. Voloshin *et al*., J. Phys. G: Nucl. Part. Phys. **34**, S883 (2007).
[40] P. K. Kovtun, D. T. Son, and A. O. Starinets, Phys. Rev. Lett. **94**, 111601 (2005).
[41] B. I. Abelev *et al*., Phys. Rev. C **77**, 054901 (2008).
[42] J. Knoll, arXiv:0803.2343 [nucl-th].
[43] E. L. Bratkovskaya, W. Cassing, and H. Stöcker, Phys. Rev. C **67**, 054905 (2003); E. L. Bratkovskaya *et al*., *ibid*. **69**, 054907 (2004).